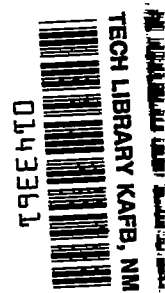


NACA RM A53H17

8179



# RESEARCH MEMORANDUM

COMPARISON OF THEORETICAL AND EXPERIMENTAL ZERO-LIFT  
DRAG-RISE CHARACTERISTICS OF WING-BODY-TAIL  
COMBINATIONS NEAR THE SPEED OF SOUND

By George H. Holdaway

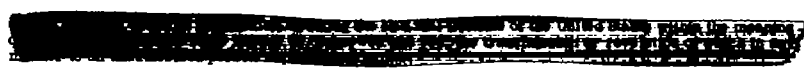
Ames Aeronautical Laboratory  
Moffett Field, Calif.

Classification cancelled (or changed to) *UNCLASSIFIED*  
By Authority of *NASA Tech. Pub. Announcement # 21*  
(OFFICER AUTHORIZED TO CHANGE)

By *H. H. 57*  
NAME AND

*N.A.S.*  
GRADE OF OFFICER MAKING CHANGE)

*30 Mar 61*  
DATE



## NATIONAL ADVISORY COMMITTEE FOR AERONAUTICS

WASHINGTON  
October 16, 1953

~~CONFIDENTIAL~~

## NATIONAL ADVISORY COMMITTEE FOR AERONAUTICS

RESEARCH MEMORANDUMCOMPARISON OF THEORETICAL AND EXPERIMENTAL ZERO-LIFT  
DRAG-RISE CHARACTERISTICS OF WING-BODY-TAIL  
COMBINATIONS NEAR THE SPEED OF SOUND

By George H. Holdaway

## SUMMARY

The zero-lift drag rise at low supersonic speeds computed by linearized theory for several wing-body-tail combinations is compared with experimental data. The experimental data were obtained by the free-fall technique covering a Mach number range of  $M = 0.8$  to  $M = 1.14$ . The procedures used in the theoretical calculations are outlined in detail. The results indicate that the computation method is capable of computing the drag rise at low supersonic speeds to an accuracy of about 20 percent.

Implications of the theory with respect to the selection of area distributions which will give a drag reduction over a range of Mach numbers are examined. For cases where fuselage indentation is not feasible, calculations indicate that drag reductions may still be possible by increasing the fuselage volume in front of and behind the wing.

## INTRODUCTION

Recent experimental results (refs. 1, 2, and 3) have demonstrated that the transonic zero-lift drag rise of wing-body combinations is primarily a function of the magnitude and rate of change of cross-sectional area along the longitudinal axis. This concept was utilized in the referenced tests to reduce the drag rise by indenting the body of a wing-body combination. These experimental results may be considered to be a qualitative verification of the linear theory as developed in references 4 through 8.

The purpose of this report is to examine the quantitative relationship between the theory and experimental data from free-fall tests of several wing-body combinations. In addition, the implications of the

theory are examined with regard to modification of the area distribution of a configuration to keep the drag rise low over a selected range of transonic Mach numbers.

This investigation utilized test data covering a Mach number range of  $M = 0.8$  to  $M = 1.14$  and a Reynolds number range of 2,500,000 to 17,000,000, depending upon the wing mean aerodynamic chord of the configuration tested.

### SYMBOLS

$A_n$	dimensionless coefficients defining the magnitude of the harmonics of a Fourier sine series
$a$	speed of sound, ft/sec
$C_{D_0}$	zero-lift drag coefficient, $\frac{\text{drag at zero lift}}{qS_w}$
$\Delta C_{D_0}$	zero-lift drag-rise coefficient, $\frac{\Delta D_0}{qS_w}$
$\Delta D_0$	zero-lift drag rise at transonic speeds, lb
$d$	fuselage maximum diameter, in.
$l$	fuselage or body length, in.
$M$	Mach number, $\frac{V}{a}$
$N$	number of terms or harmonics used in the Fourier sine series
$q$	dynamic pressure, $\frac{1}{2} \rho V^2$ , lb/sq ft
$S$	projection of $S_g$ on a plane perpendicular to $x$ axis, sq in.
$S_g$	cross-sectional areas formed by cutting the configurations with perpendicular or oblique planes $X$ , sq in.
$S_w$	wing area, sq ft
$V$	free-stream velocity, ft/sec
$x$	distance along the $x$ axis measured from the midlength position, in.
$x, y, z$	Cartesian coordinates as conventional body axes

- $\theta$  angle between the  $z$  axis and the intersection of the cutting planes  $X$  with the  $yz$  plane
- $\mu$  Mach angle, arc sin  $\frac{1}{M}$
- $\rho$  mass density of air, slugs/cu ft
- $\phi$  transformation of the length  $x$  to radians, arc cos  $\frac{x}{l/2}$ , radians
- $X$  a series of parallel cutting planes intersecting the  $x$  axis at the Mach angle  $\mu$   
(At  $M = 1.0$  these planes are perpendicular to the  $x$  axis; i.e., parallel to the  $yz$  plane.)
- $\psi$  angle between the  $y$  axis and the intersection of the cutting planes  $X$  with the  $xy$  plane, arc tan  $(\sqrt{M^2-1} \cos \theta)$
- $S'$  first derivative of the projected cross-sectional area,  $\frac{dS}{dx}$
- $S''$  second derivative of the projected cross-sectional area,  $\frac{d^2S}{dx^2}$

## THEORY

### Development of the Theory

Contributions to the development of the theory were made by the investigations reported in references 4 through 8. The calculated drag rise of slender bodies of revolution and the analogy between the drag-rise equations and the induced-drag equations for a wing are presented in reference 4. The development of equations for bodies of revolution with minimum drag rise is presented in reference 5 which also illustrates the application of a sine series to evaluate the theoretical drag rise. The theory was extended to arbitrary systems in reference 6, which showed how these arbitrary systems could be represented by equivalent bodies of revolution. This latter theory was applied to lifting surfaces in references 7 and 8.

The application (and limitations) of these methods to the theoretical computation of the drag rise of wing-body combinations is presented in reference 9. The methods of reference 9 were used to make the theoretical calculations for this report. The theory merely applies to the wave drag; any local shock or separation effects which might occur due to shape modification were not evaluated in the development of the theory.

~~CONFIDENTIAL~~

### Concepts Leading to the Drag Equation

The derivation of the drag equation for a wing-body-tail combination is based on the theory that the configuration may be represented by a series of equivalent bodies of revolution. This theory is dependent on a simplified relationship between source strength and cross-sectional area. This relationship is used in planar wing and slender body of revolution problems. Specifically, as was pointed out in reference 9, the source strength is assumed to be proportional to the normal component of the stream velocity at the body surface. The theory also assumes that the configuration is of a conventional type with thin symmetrical airfoil surfaces and a high fineness ratio body. Further exceptions and limitations to the theory are given in reference 9.

The development of equivalent bodies of revolution will be illustrated by using the configuration shown in figure 1. The wing-body-tail combination is cut by a series of planes which always intersect the longitudinal axis at the Mach angle  $\mu$ . In other words, these planes are tangent to Mach cones. The plane identified in figure 1 as  $X_1$  represents one plane of a series of parallel planes which cut the configuration along the entire longitudinal axis. Each plane of this series intercepts the  $yz$  plane in a line which forms the angle  $\theta_1 = 0^\circ$  with the  $z$  axis. Similarly, planes  $X_2$  form the angles  $\theta_2$  with the  $z$  axis and the  $yz$  plane. For any one cutting plane of the series of planes  $X_2 = f(\theta_2, \mu)$  the oblique cross-sectional area is projected on a plane perpendicular to the  $x$  axis. This projected cross-sectional area is plotted as a function of  $x$ . The resulting plot may be considered as representing the longitudinal distribution of cross-sectional area  $S(x)$  of an equivalent body of revolution for the series of planes  $X_2 = f(\theta_2, \mu)$ . For any one value of  $\mu$  this process is repeated for other values of  $\theta$  ranging from  $\theta = 0$  to  $\theta = 2\pi$ . However, if the configuration is symmetrical with respect to the  $xy$  and  $xz$  planes, then equivalent bodies for  $\theta$  from 0 to  $\pi$  only need be obtained. For bodies of revolution the area distribution is independent of  $\theta$ .

With these concepts and with the use of the simplified relationship between source strength and cross-sectional area, the equation for the zero-lift drag rise as a function of the rate of change of cross-sectional area can be derived from equation (46) of reference 7 and written as:

$$\Delta D_0 = - \frac{\rho V^2}{8\pi^2} \int_0^{2\pi} \int_0^l \int_0^l S''(x_1) S''(x_2) \ln|x_1 - x_2| dx_1 dx_2 d\theta \quad (1)$$

where  $x_1$  and  $x_2$  are two different locations along the  $x$  axis,

$$S''(x) = \frac{d^2 S(x)}{dx^2} \quad (2)$$

This generalized equation can be simplified by solving the double integral of the functions of  $x$  through a Fourier sine series in the same manner as used in reference 5.

$$\int_0^l \int_0^l S''(x_1) S''(x_2) \ln|x_1 - x_2| dx_1 dx_2 = -\frac{1}{144} \frac{\pi^2}{2} \left(\frac{l}{2}\right)^2 \sum_{n=1}^N n A_n^2 \quad (3)$$

(The factor 144 appears because the body length,  $l$ , has been defined in inches for this report.)

Where

$$S'(x) = \frac{dS}{dx} = \frac{l}{2} \sum_{n=1}^N A_n \sin n\varphi \quad (4)$$

and

$$\varphi = \arccos \frac{x}{l/2} \quad (5)$$

then

$$A_n = \frac{2}{\pi} \frac{2}{l} \int_0^\pi S'(x) \sin n\varphi d\varphi \quad (6)$$

where the coefficients are a function of  $\theta$ , since  $S'(x)$  is a function of  $\theta$ . With this solution the simplified equation can now be written as

$$\Delta D_0 = \frac{1}{144} \frac{\rho V^2}{2} \left(\frac{l}{2}\right)^2 \frac{1}{8} \int_0^{2\pi} \sum n A_n^2 d\theta \quad (7)$$

The computing procedure followed in applying the foregoing equations and theory to the determination of the zero-lift drag rise is presented in the Appendix of this report.

#### CONFIGURATIONS AND TESTS

Plan-view sketches of the models tested, and also the axial distribution of cross-sectional area normal to the longitudinal axis, are shown in figure 2. The different configurations will be referred to as models A, B, C, and D as follows:

Model A: aspect ratio 4 triangular wing with fuselage and tail

Model B: aspect ratio 3 straight wing with fuselage and tail

~~CONFIDENTIAL~~

Model C: aspect ratio 6, 45° sweptback wing with fuselage and tail

Model D: fuselage and tail (consisting of two vertical and two horizontal surfaces)

General geometric data for all the models are presented in table I, with greater detail given for model D in figure 3. The fuselage and tail were the same for all models. The fuselage ordinates from the 8-inch to the 139.4-inch station are given by the equation shown in figure 3. All cross sections of the fuselage were circular, and the nose of the fuselage was faired from the ordinate at the 8-inch station down to a 1-1/2-inch-diameter boom 15 inches forward of that station. The fuselage was not indented.

The free-fall technique employed is described in detail in reference 10. The tests covered a Mach number range of 0.8 to 1.14 and had approximately the following Reynolds number variation:

<u>Model</u>	<u>M = 0.8</u>	<u>M = 1.1</u>
A	7,500,000	16,600,000
B	5,750,000	12,400,000
C	2,600,000	5,600,000
D	35,800,000	77,000,000

The values of Reynolds number for models A, B, and C are based on the wing mean aerodynamic chords, and the values for model D are based on the fuselage length of 210.5 inches.

The accuracy of the measurements of the drag rise divided by  $q$  and the Mach number is believed to be within  $\frac{\Delta D_0}{q} = \pm 0.06$  and  $M = \pm 0.01$ .

Without an attempt to evaluate here the accuracy or limitations of linearized theory, the theoretical computations as made are estimated to be accurate within 2 percent, except where linear theory might indicate a singularity in the drag curve. This accuracy of the theoretical data is based upon approximate methods for integrating the areas and determining the slopes of the area plots. Greater accuracies might be obtained by methods more exact than those outlined in the Appendix but probably are not justified.

## RESULTS

The experimental zero-lift drag coefficients for the four models are presented in figure 4. The drag coefficients are based on the wing areas for models A, B, and C, and the fuselage maximum cross-sectional area for model D. The incremental drag rises above the subsonic values at  $M = 0.8$

are presented in figure 5, together with the results of the theoretical computations. The rather large differences in wing area make comparison between configurations difficult; therefore, the data of figure 5 were multiplied by the respective areas used in computing the drag coefficients and the results presented in figure 6. The apparent late drag rise for model A is attributed to possible error in fairing the experimental data points which had scatter equal to  $\frac{\Delta D_0}{q} = 0.06$  from the mean.

## DISCUSSION

### Agreement Between Experiment and Theory

Comparison of the drag-rise values presented in figure 6 indicates that, in general, the theoretical computations give a good prediction of the experimental values. Limitations in the theory resulted in only qualitative agreement being obtained between theory and experiment at Mach numbers below about 1.02. At Mach number 1.0 the experimental drag rise is less than the theoretical value, varying from 46 to 74 percent of theory. It may be noted that the greater the departure of the configuration from that of a body of revolution the greater the difference between theory and experiment became for  $M = 1.0$ .

For Mach numbers greater than 1.0, the effect of theory limitations is diminished and the level of the drag rise is predicted quantitatively. In general, the values above  $M = 1.02$  are in error by about 20 percent with a maximum deviation of experiment from theory of 26 percent.

### Application of Theory

The prior section illustrated the adequacy of the theory in estimating the zero-lift drag rise of wing-body-tail combinations. It is of interest next to examine the implications of the theory with regard to possible drag reductions through modifications of the area distribution.

Consider a design problem involving a configuration similar to model B with an engine or other components within the fuselage which might make fuselage indentation impractical. In a case such as this the drag reduction would have to be attempted by adding volume before and behind the wing. That such an approach might be successful is illustrated in figure 7(a). The solid curve is the computed drag rise for the unmodified configuration. The lowest, straight line represents the theoretical drag rise for a Sears-Haack body with the same maximum cross-sectional area as the wing-body combination. The large difference between these two curves suggests the possibility of reducing the drag

rise of the original configuration by modifying its area distribution to approach, as a limit, the Sears-Haack distribution.

The modification curves presented in figure 7(b) represent various fuselage revisions, obtained by adding volume to the fuselage in front of and behind the wing. Modification 1 is similar to the type of fuselage revision discussed in reference 1, in that it is based entirely on the distribution of cross-sectional area perpendicular to the  $x$  axis. Such a revision would be expected to reduce the drag rise at a Mach number of 1.0, and this anticipation is realized in figure 7(a). However, the desired equivalent body of revolution for  $M = 1.0$  is not the desired shape for other Mach numbers, and a rapid rise in drag with increasing Mach number therefore results as shown in figure 7(a). This drag rise is independent of possible separation effects which were not evaluated in the theory used.

Clarification of the above point is afforded by consideration of figure 8(a). On this figure are shown the projected cross-sectional area distributions ( $S$ ) of the original wing-fuselage-tail configuration for various angles  $\psi_{\max}$ . The largest angle  $\psi_{\max}$  is used for each Mach number computation and is the complement of the Mach angle. (The equivalent tail area for the larger angles showed only slight differences from the  $\psi_{\max} = 8.08^\circ$ , so was omitted from this figure for clarification. The fuselage having a high fineness ratio had essentially the same area distribution for the entire Mach number range.) Shown on figure 8(a) is also a Sears-Haack body area distribution for a body with maximum cross-sectional area equal to that of the original wing plus body. Modification 1, which optimizes the area distribution on the original wing-fuselage combination for a Mach number of 1.0, consists of additions to the body cross-sectional area sufficient to fill in the difference indicated by the shaded area. The fact that excess area is added for other Mach numbers is indicated by the penetration of the ( $S$ ) curves for other values of  $\psi_{\max}$  into this shaded area. If it is desired to reduce the drag at Mach numbers somewhat above 1.0, much less volume should be added to the regions immediately in front of and behind the wing.

In arriving at such a compromise for the wing body under consideration, the following approach was followed to establish the lines for modification 2. The five area distributions ( $S$ ) shown in figure 8(a) were arbitrarily replaced by a single curve representing the arithmetic average of the five curves. The Sears-Haack body area distribution was modified to represent a Sears-Haack body having a maximum cross-sectional area equal to the maximum of this averaged curve. The volume added to the fuselage was determined from the difference between this new Sears-Haack body curve and the average curve as shown in figure 8(b). The  $\psi_{\max}$  curves for  $M = 1.0$  and  $M = 1.14$  are also shown on figure 8(b) to illustrate the reduction in the size of the new Sears-Haack body as well as the reduction in volume to be added immediately before and behind the wing. The computed drag rise for this second modification (fig. 7(a))

shows an improvement in comparison to the original unmodified configuration over the entire design Mach number range of from 1.0 to 1.14.

Modifications 3 and 4 were derived by the method described in reference 9 for the design of a fuselage modification optimized for a specific Mach number. Mach numbers of 1.05 and 1.14 were arbitrarily selected and the results of the calculations are presented in figures 7(a) and 7(b). Modification 3 produced only a slight improvement over modification 2, but it was maintained over the Mach number range shown. Apparently, as the minimum drag curve for a configuration is approached, slight streamwise modifications to the fuselage about the optimum shape can be made without greatly changing the drag. Further reduction of the drag rise at the higher Mach numbers at the expense of an increase at the lower Mach numbers could probably be effected by optimizing for the highest operating Mach number as was done in modification 4. Due to the limitations of the drag computations near Mach number 1.0, experimental investigations should be made to see if these small drag differences for modifications 3 and 4 really do exist.

#### CONCLUSIONS

The results of the computations and experimentation presented in this report indicate that for the models tested the following conclusions are justified:

1. A computation method has been established which is capable of predicting the zero-lift drag rise at low supersonic speeds for a wide variety of wing-fuselage-tail combinations within an accuracy of about 20 percent.
2. In establishing the modifications to be made to a fuselage to reduce the drag rise, the effect of various revisions should be examined for a range of Mach numbers.
3. For cases where fuselage indentation is not feasible, theory indicates that drag reductions may still be possible by increasing the fuselage volume in front of and behind the wing.

Ames Aeronautical Laboratory  
National Advisory Committee for Aeronautics  
Moffett Field, Calif., Aug. 17, 1953

## APPENDIX

## PROCEDURE USED FOR COMPUTING ZERO-LIFT DRAG RISE

The detailed application of the drag equation developed in the theoretical section of this report is outlined in the following paragraphs. The general procedures are presented with various simplifications and suggested methods based on experience gained in making the computations for this report. The simplest case is presented first in order to better illustrate the basic steps and to shorten the presentation of the more involved procedures.

Calculation at  $M = 1.0$  for both Symmetrical and  
Unsymmetrical Configurations

At  $M = 1.0$  the cutting planes  $X$  are perpendicular to the  $x$  axis and the projected cross-sectional areas are independent of the angle  $\Phi$ . Therefore, the drag rise at  $M = 1.0$  is computed in the same manner for symmetrical or unsymmetrical configurations.

Step 1.- Determine the total cross-sectional area of the wing-body-tail combination and plot the area distribution as shown in figure 9(a).

Step 2.- Differentiate the area plot, figure 9(a), with respect to  $x$ , and plot the results as a function of  $\Phi$  as is indicated in figure 9(b). The technique of reference 11 may be used to differentiate the area curve.

Step 3.- Fit a Fourier sine series to the curve of figure 9(b) in order to determine the magnitude of the coefficients of the various harmonics. For example, from equation (6) of the theoretical section the coefficients  $A_n$  are computed as follows:

$$A_1 = \frac{4}{\pi l} \int_0^\pi \frac{dS}{dx} \sin \Phi d\Phi$$

$$A_2 = \frac{4}{\pi l} \int_0^\pi \frac{dS}{dx} \sin 2 \Phi d\Phi, \text{ etc.}$$

The integrations may be accomplished by punch card machine computation, electronic-wave-analysis equipment or by ordinary long-hand computing methods. However, early investigations in connection with the computations made for this report showed that a large number of terms (over 12) would be required to fit the irregular curves normally obtained, which

would rule out long-hand computing methods. Available electronic-wave-analysis equipment gave the relative magnitude of the coefficients but not their absolute values. The punch card computing methods were used for this report. Practical considerations of over-all accuracy did not justify calculating for more than 24 harmonics. On the other hand, computing for less than 12 harmonics reduced the resultant theoretical drags as much as 40 percent for some of the configurations investigated in this report.

Step 4.- Compute the drag rise from equation (7) which for  $M = 1.0$  reduces to the following coefficient form:

$$\Delta C_{D_0} = \frac{\pi}{576 S_w} \left(\frac{l}{2}\right)^2 \sum_{n=1}^{n=24} n A_n^2$$

In using equations (6) and (7) they may be simplified by deleting  $2/l$  and  $(l/2)^2$ , respectively, provided  $A_n$  is considered as a dimension in inches.

Calculation for Mach Number Range, Configuration Symmetrical  
With Respect to  $xy$  and  $xz$  Planes, Wings  
and Tail Surfaces in  $xy$  Plane Only

The first three steps in this calculation are essentially the same as for the  $M = 1.0$  calculation except the computations should be made for at least four equivalent bodies of revolution rather than for just one.

Step 1.- Select the Mach number range to be covered by the computations and determine the cross-sectional areas of the equivalent bodies of revolution for each value of  $\theta$  ( $\mu = \text{constant}$ ) and plot as shown in figure 9(a). By judicious selection of cutting planes for the computation of the drag for the highest Mach number, the drag at lower Mach numbers can be computed from the same cross sections. This means that the values of  $\psi_{\max}$  used for the lower Mach numbers are used for the intermediate values of  $\psi$  for the higher Mach numbers. For thin airfoil surfaces, which for purposes of this computation may be assumed to lie in the  $xy$  plane, the surfaces may be cut at angles  $\psi$  by planes perpendicular to the  $xy$  plane. The actual obliqueness or error in the wing cross sections disappears as the areas are projected onto the  $yz$  plane. It should be recalled that  $\psi$  is the intercept angle of a  $\theta$  plane with the  $xy$  plane. The prior statements can be illustrated by an example showing the angles  $\psi_{\max}$  which might be used in determining the cross sections for computations for  $M = 1.30$ .

$$\psi_{\max} = \arcsin \sqrt{M^2 - 1}$$

<u>M</u>	<u><math>\psi_{\max}</math>, deg</u>
1.00	0
1.01	8.08
1.02	11.38
1.05	17.75
1.14	28.70
1.30	39.71

The equivalent bodies of revolution are determined for each of the above angles by cutting the configuration by a family of parallel planes. Then the area for each cross section is projected onto the  $yz$  plane by multiplying the area by  $\cos \psi_{\max}$ . This produces the equivalent bodies of revolution used in the final computations, where the drag computations for  $M = 1.05$  will use only the equivalent bodies for the first four angles.

For high fineness ratio fuselages, it is not necessary to cut the fuselage at various angles, because the projection of the cross-sectional areas onto the  $yz$  plane results in essentially a constant area distribution with Mach number as mentioned previously. For a fixed area distribution, the shape of the cross section of a high fineness ratio body is relatively unimportant if the body ends in a cylinder or a point (see ref. 12). The zero-lift drag-rise coefficients for the Sears-Haack bodies can be computed from equation (14), reference 5, which illustrates that the supersonic drag is constant:

$$\Delta C_{D_0} = \frac{9}{8} \pi^2 \left( \frac{d}{l} \right)^2$$

Step 2.- Differentiate the area plots and plot as a function of  $\psi$  as indicated in figure 9(b).

Step 3.- Fit a Fourier sine series to the curves of the area plots in the same manner as for the  $M = 1.0$  computations.

Step 4.- For the largest Mach number and angles  $\psi$ , compute the angles  $\theta$  and plot  $\sum n A_n^2$  as shown in figure 9(c). The same data can be used for the intermediate Mach numbers as follows:

M = 1.14			M = 1.05			M = 1.02		
$\psi$ , deg	$\theta$ , radian	$\Sigma n A_n^2$	$\psi$ , deg	$\theta$ , radian	$\Sigma n A_n^2$	$\psi$ , deg	$\theta$ , radian	$\Sigma n A_n^2$
0	1.571	90	0	1.571	90	0	1.571	90
8.08	1.285	70	8.08	1.092	70	8.08	.787	70
8.08	1.857 <sup>a</sup>	70	8.08	2.050	70	8.08	2.355	70
11.38	1.173	60	11.38	.890	60	11.38	0	60
11.38	1.969 <sup>a</sup>	60	11.38	2.252	60	11.38	3.142	60
17.75	.946	50	17.75	0	50			
17.75	2.196 <sup>a</sup>	50	17.75	3.142	50			
28.70	0	45						
28.70	3.142 <sup>a</sup>	45						

<sup>a</sup>Angles  $\theta$  are taken symmetrical about  $\theta = \pi/2$ .

Step 5.- Integrate the area under curves similar to figure 9(c) and compute the drag-rise coefficient from the following equation derived from equation (7):

$$\Delta C_{D_0} = \frac{1}{576 S_w} \left( \frac{l}{2} \right)^2 \int_0^\pi \sum_{n=1}^{n=24} n A_n^2 d\theta$$

Calculation for Mach Number Range, Configuration Symmetrical  
With Respect to xy and xz Planes, Wings  
and Tail Surfaces in Both Planes

The essential differences from the prior method is that the vertical surfaces are rotated  $90^\circ$  into the xy plane, and if the same values of  $\psi$  used for the cutting of the horizontal surfaces are used to cut vertical surfaces then the cross sections for the vertical surfaces will correspond to different angles  $\theta$  than those used for the horizontal surfaces. Because the areas must be combined to give an equivalent body of revolution for one value of  $\theta$ , cross plots of the areas should be made or the vertical surfaces should be cut at different angles than the horizontal surfaces. A satisfactory and simple procedure is to cut the vertical surfaces for one or two angles more than the horizontal surfaces to ensure a uniform variation of angles from  $0$  to  $90^\circ$ , and then proceed as follows:

Step 1.- Multiply the cross-sectional areas for the vertical surfaces by  $\cos \psi$ .

Step 2.- For each fuselage station plot the areas from step 1 as a function of  $\theta_V = \theta_H - 90^\circ$ . Subscripts V and H refer to the vertical and horizontal surfaces, respectively.

~~CONFIDENTIAL~~

Step 3.- Read the areas from step 2 that correspond to the values of  $\theta$ .

Step 4.- Combine the cross-sectional areas (already multiplied by  $\cos \psi$ ) for the vertical and horizontal surfaces to give one equivalent body for one angle  $\theta_H = \theta$ .

Step 5.- Compute the drag-rise coefficients as before for the case where all surfaces were in the  $xy$  plane.

#### Calculation for Mach Number Range, Unsymmetrical Configuration

This calculation is similar to the prior method except that the final integration must be performed from  $\theta = 0$  to  $\theta = 2\pi$  and the equivalent bodies of revolution determined from negative angles of  $\psi$  as well as from positive angles. These factors lengthen the problem but do not add to the complexity.

#### Time to Perform Calculations

Computations for this report, as was mentioned previously, were made by punch card machine computations. Time to compute the drag rise for a wing, similar to the models tested for this report, in combination with a high fineness ratio body from  $M = 1.0$  to  $M = 1.2$ , was found to require approximately 80 computer hours. This value is based on experience gained in making the computations for this report and includes the time to lay out the cross sections and integrate the areas graphically.

## REFERENCES

1. Whitcomb, Richard T.: A Study of the Zero-Lift Drag-Rise Characteristics of Wing-Body Combinations Near the Speed of Sound. NACA RM L52H08, 1952.
2. Williams, Claude V.: A Transonic Wind-Tunnel Investigation of the Effects of Body Indentation, as Specified by the Transonic Drag-Rise Rule, on the Aerodynamic Characteristics and Flow Phenomena of an Unswept Wing-Body Combination. NACA RM L52L23, 1953.
3. Robinson, Harold L.: A Transonic Wind-Tunnel Investigation of the Effects of Body Indentation, as Specified by the Transonic Drag-Rise Rule, on the Aerodynamic Characteristics and Flow Phenomena of a  $45^\circ$  Sweptback-Wing-Body Combination. NACA RM L52L12, 1953.
4. von Kármán, Th.: The Problems of Resistance in Compressible Fluids (Fifth Volta Congress) Tema, Reale Accademia D'Italia, 1936.
5. Sears, William R.: On Projectiles of Minimum Wave Drag. Quart. of Appl. Math., vol. IV, no. 4, Jan. 1947, pp. 361-366.
6. Hayes, Wallace D.: Linearized Supersonic Flow. North American Aviation, Inc., Rep. No. AL-222, 1947.
7. Heaslet, Max. A., Lomax, Harvard, and Spreiter, John R.: Linearized Compressible-Flow Theory for Sonic Flight Speeds. NACA Rep. 956, 1950.
8. Jones, Robert T.: Theoretical Determination of the Minimum Drag of Airfoils at Supersonic Speeds. Jour. Aero. Sci., vol. 19, no. 12, Dec. 1952, pp. 813-822.
9. Jones, Robert T.: Theory of Wing-Body Drag at Supersonic Speeds. NACA RM A53H18a, 1953.
10. Holdaway, George H.: Comparison of the Aerodynamic Characteristics at Transonic Speeds of a Plane Wing and a Cambered and Twisted Wing, Both Having  $45^\circ$  of Sweepback and an Aspect Ratio of 6. NACA RM A53B16, 1953.
11. Kauffman, William M., and Shinbrot, Marvin: A Method for Differentiation of Experimental Data. Readers Forum, Jour. Aero. Sci., vol. 20, no. 6, June 1953, pp. 428-430.
12. Graham, Ernest W.: The Pressure on a Slender Body of Non-Uniform Cross-Sectional Shape in Axial Supersonic Flow. Douglas Aircraft Co., Inc., Rep. No. SM-13346A, July 1949.

TABLE I.- DIMENSIONS OF TEST MODELS

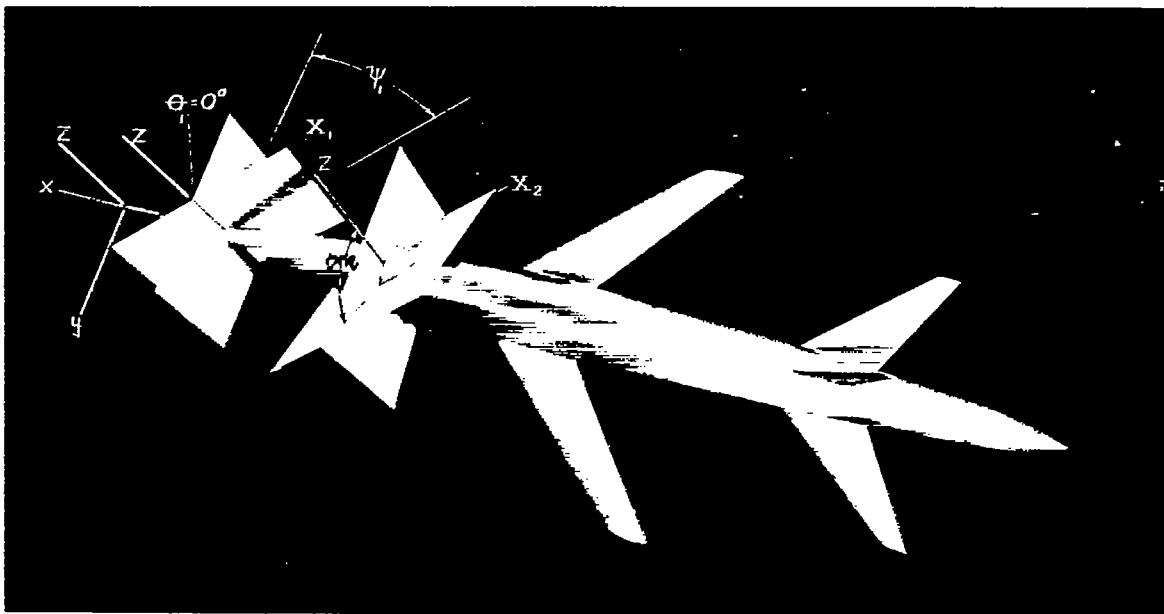
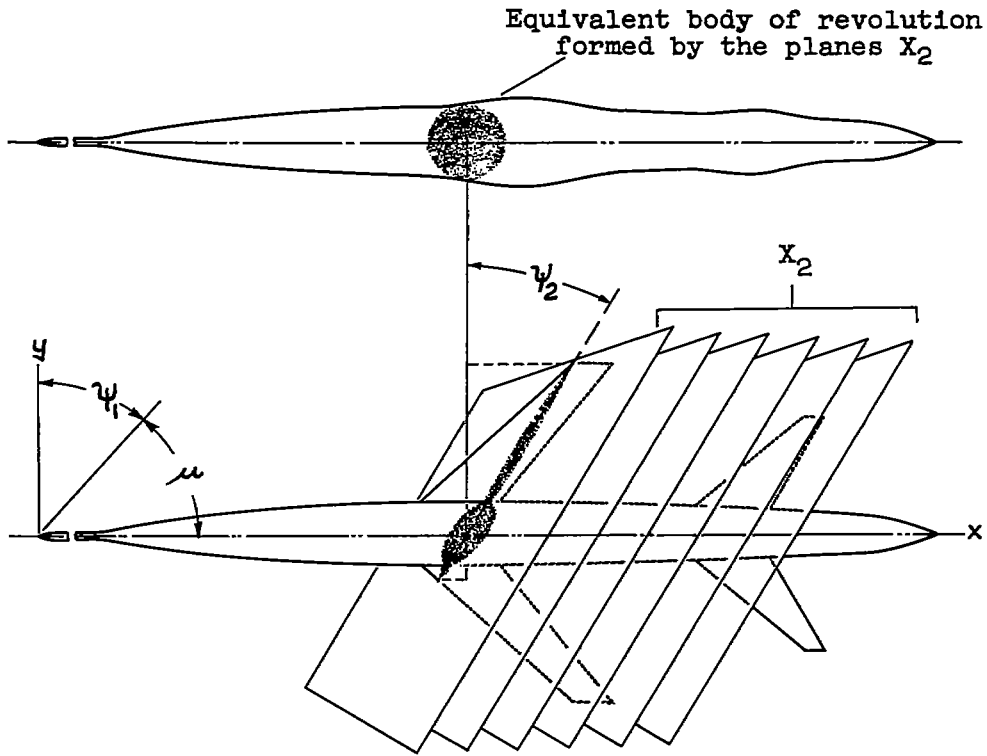
(a) Wings<sup>1</sup>

	Model A	Model B	Model C
Area, sq ft	30.07	21.68	9.02
Mean aerodynamic chord, ft	3.656	2.813	1.272
Wing span, ft	10.97	8.20	7.36
Aspect ratio	4	3.1	6
Taper ratio	0	0.39	0.5
Airfoil section	NACA 0005-63	0 to 0.5c Ellipse 0.5 to 1.0c Biconvex t/c = 3 percent	NACA 64A010 perpendicular to 0.25 chord
Sweep of 0.25 chord	(Leading edge) 45°	0°	45°
Twist, dihedral and incidence, deg	0	0	0

(b) Fuselage and tails for models A, B, C, and D<sup>2</sup>

Fuselage	
Fineness ratio . . . . .	12.4
Maximum diameter, ft . . . . .	1.417
Nose boom diameter, in. . . . .	1.5
Horizontal surfaces	
Area, sq ft . . . . .	6.0
Aspect ratio . . . . .	4.5
Taper ratio . . . . .	0.20
Airfoil section . . . . .	NACA 65006 streamwise
Sweep of 0.25 chord . . . . .	45°
Vertical surfaces	
Area, sq ft . . . . .	3.3
Aspect ratio . . . . .	5.1
Taper ratio . . . . .	0.22
Airfoil section . . . . .	NACA 65009 perpendicular to 0.25 chord
Sweep of 0.25 chord . . . . .	45°

<sup>1</sup>See figure 2.<sup>2</sup>See figure 3.



18459

Figure 1.- Illustration of the cutting planes  $X$  and the angles  $\phi$  and  $\psi$ , which are the intercepts of these planes with the  $yz$  and  $xy$  planes, respectively.

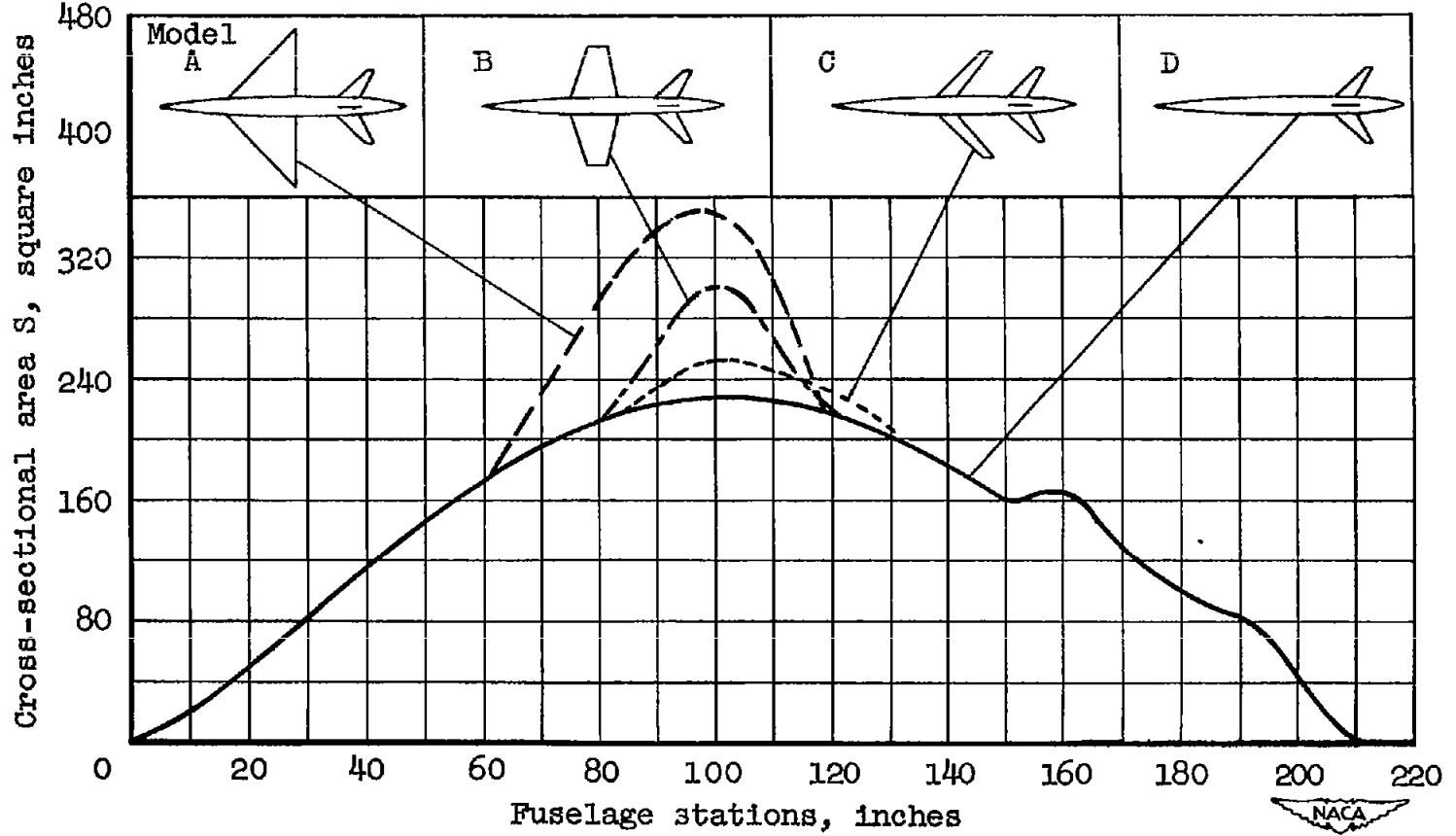
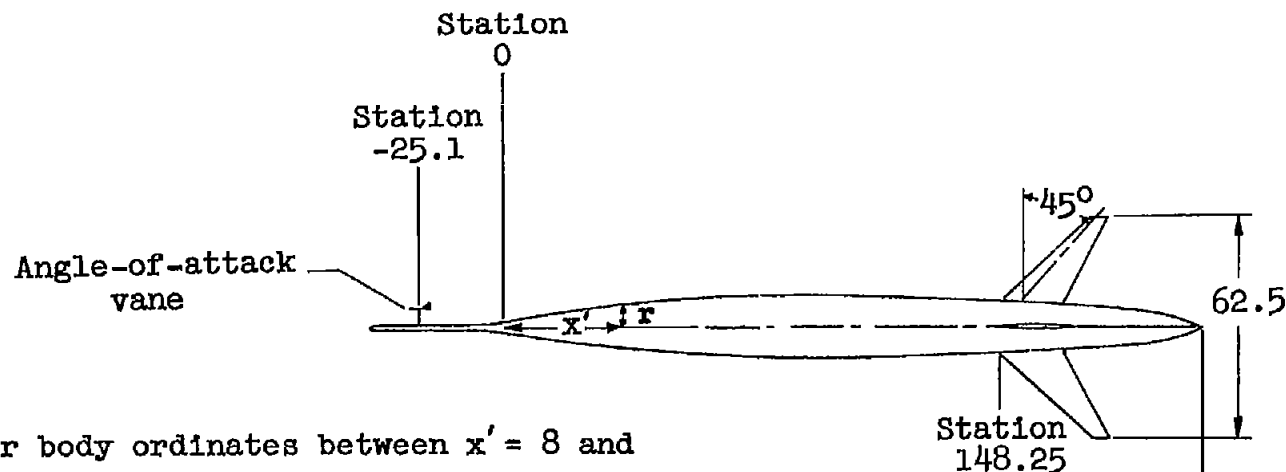


Figure 2.- Plan views of the models tested shown with their axial distributions of cross-sectional area normal to the longitudinal axis.

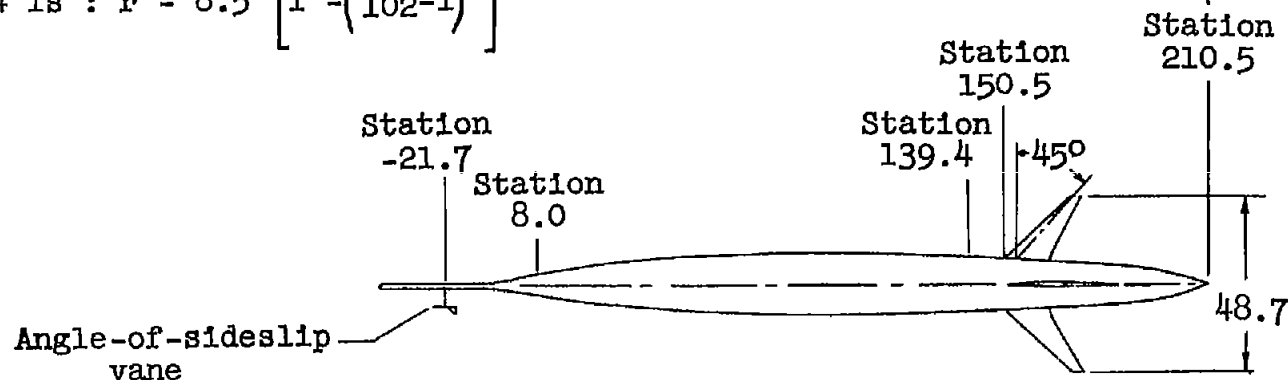
Plan view



Equation for body ordinates between  $x' = 8$  and

$$x' = 139.4 \text{ is : } r = 8.5 \left[ 1 - \left( \frac{x'}{102} - 1 \right)^2 \right]^{3/4}$$

Side view



Note: All dimensions are in inches.

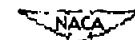


Figure 3.- Geometry and dimensions of model D.

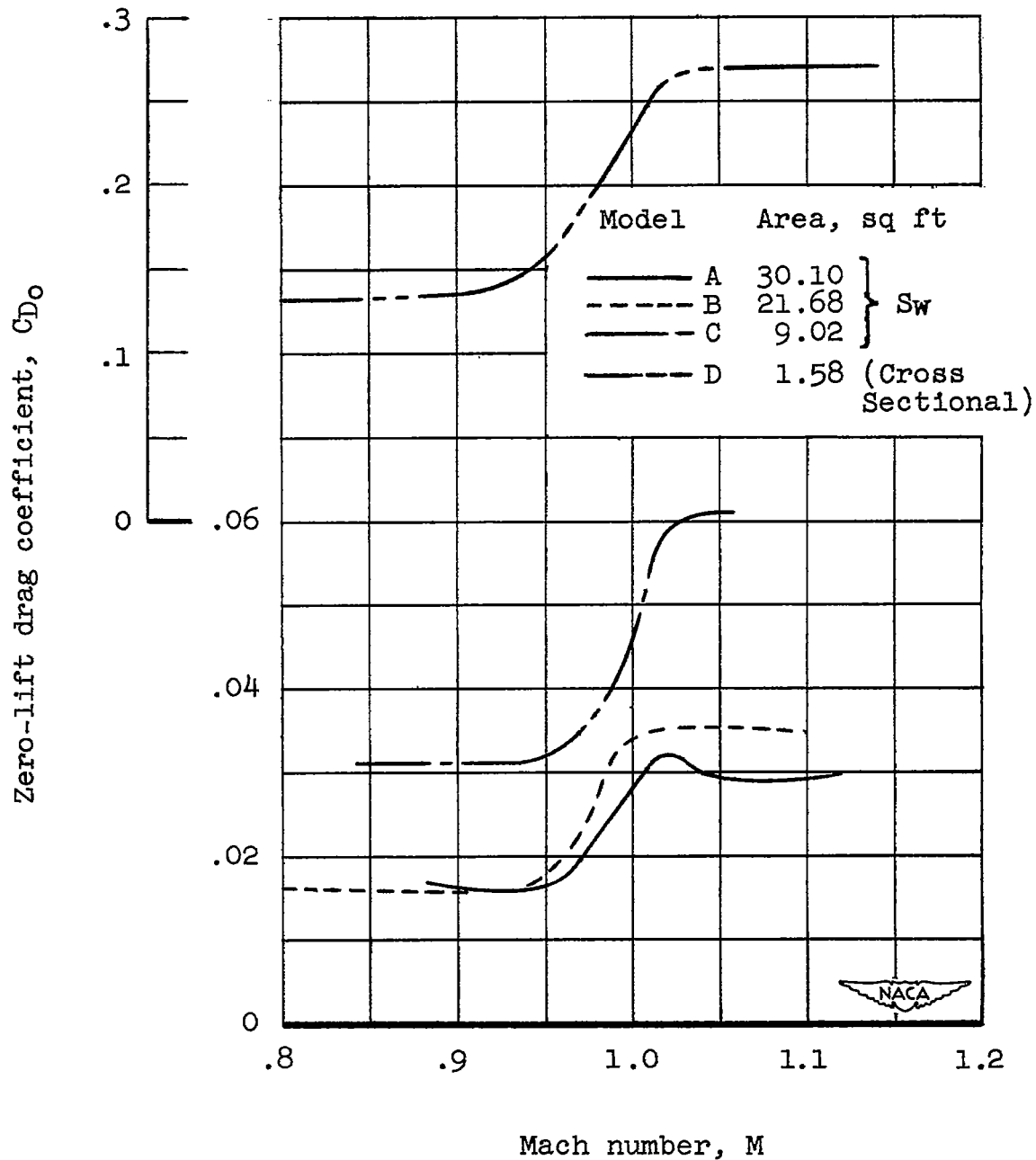


Figure 4.- Experimental zero-lift drag coefficients, based upon wing area for models A, B, and C and upon maximum cross-sectional area for model D.

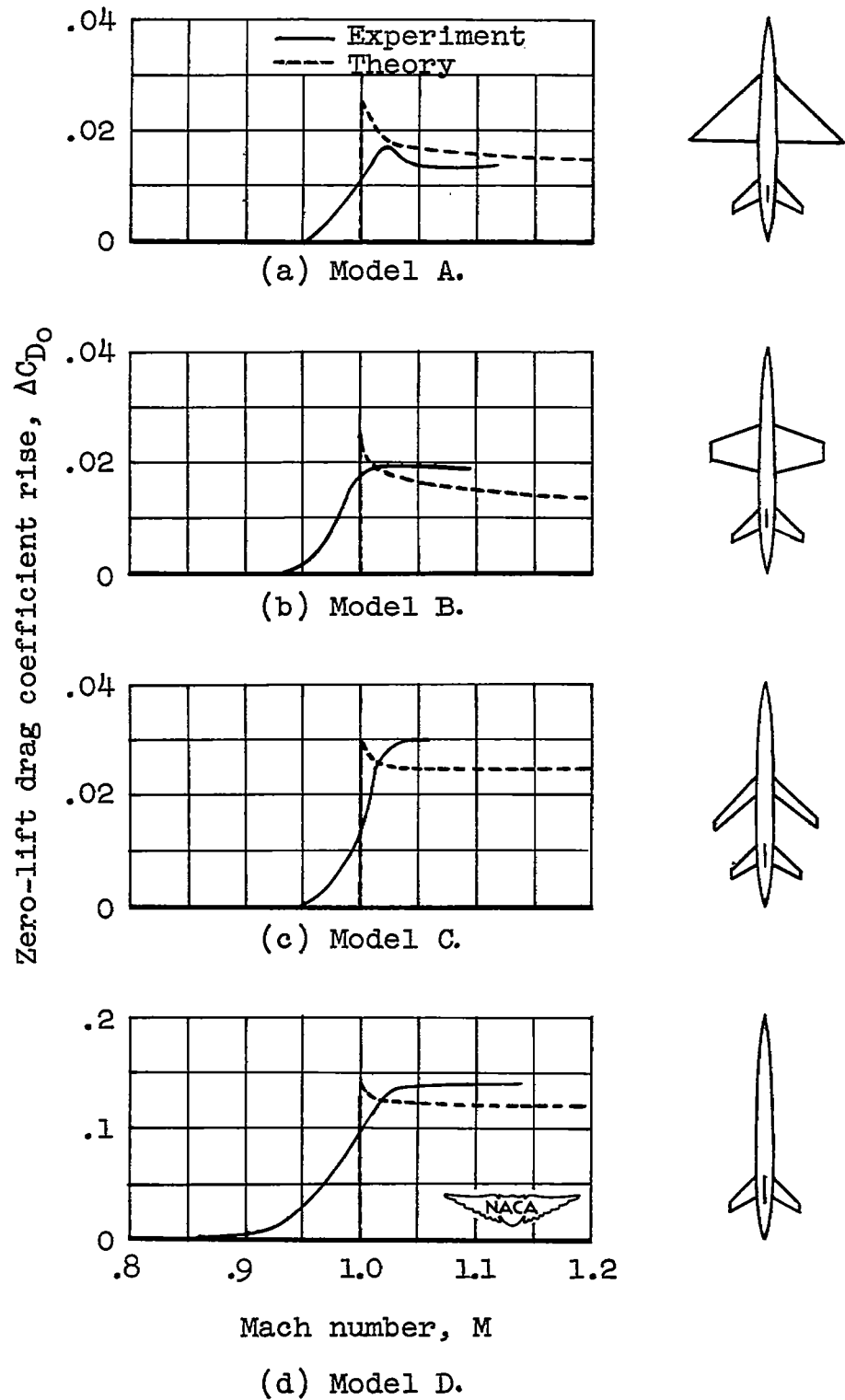


Figure 5.- Comparison of experimental drag rises with values calculated utilizing linearized theory.

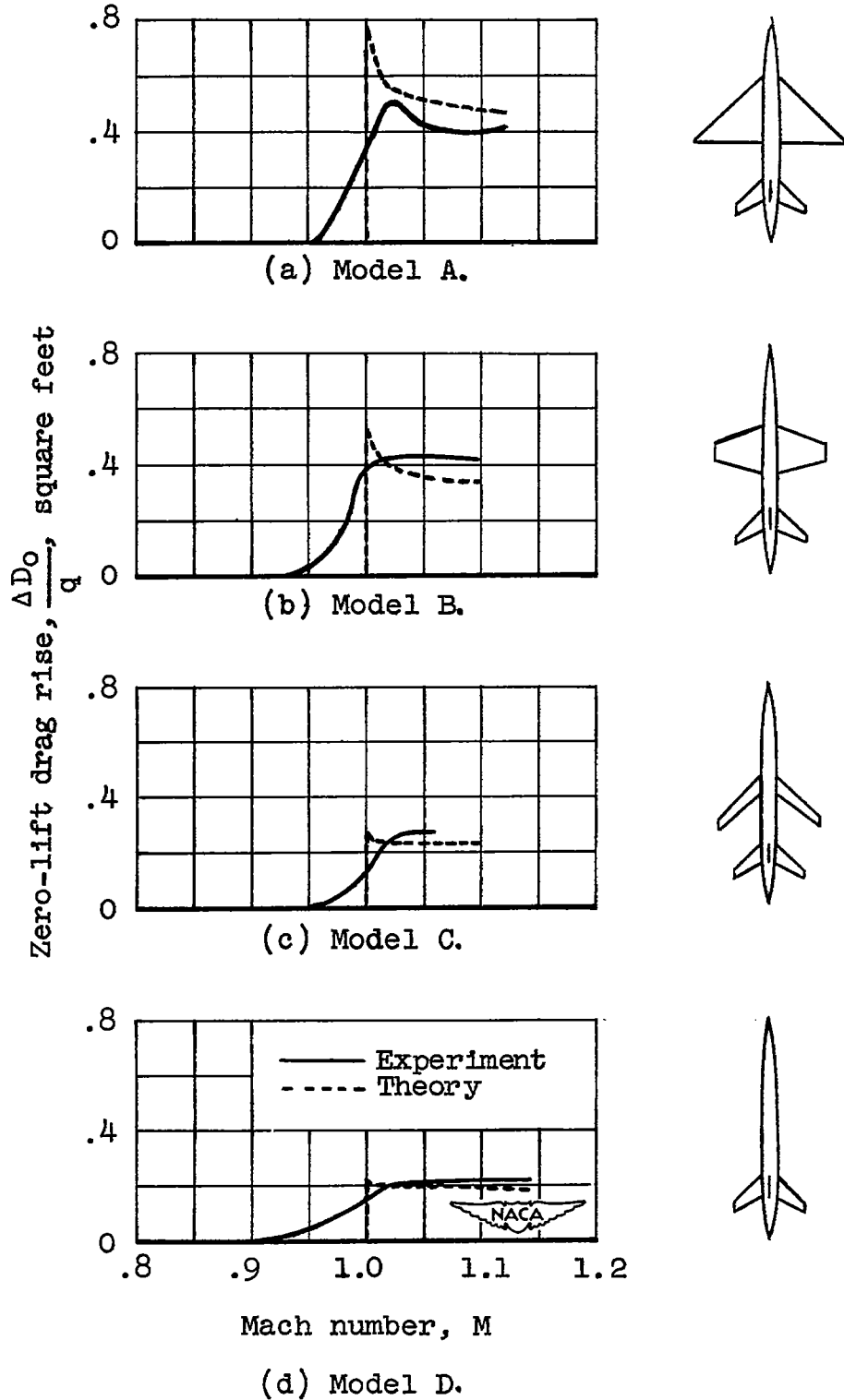
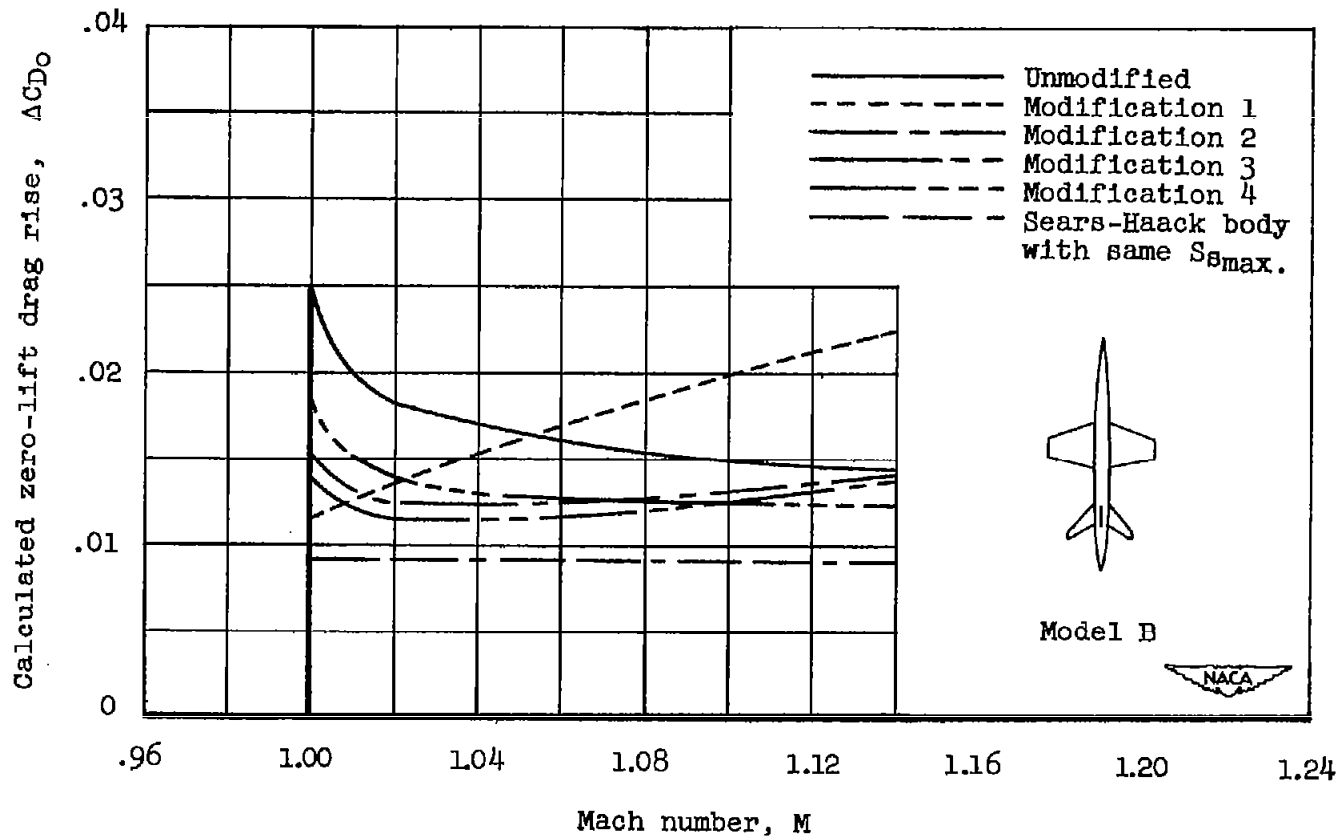


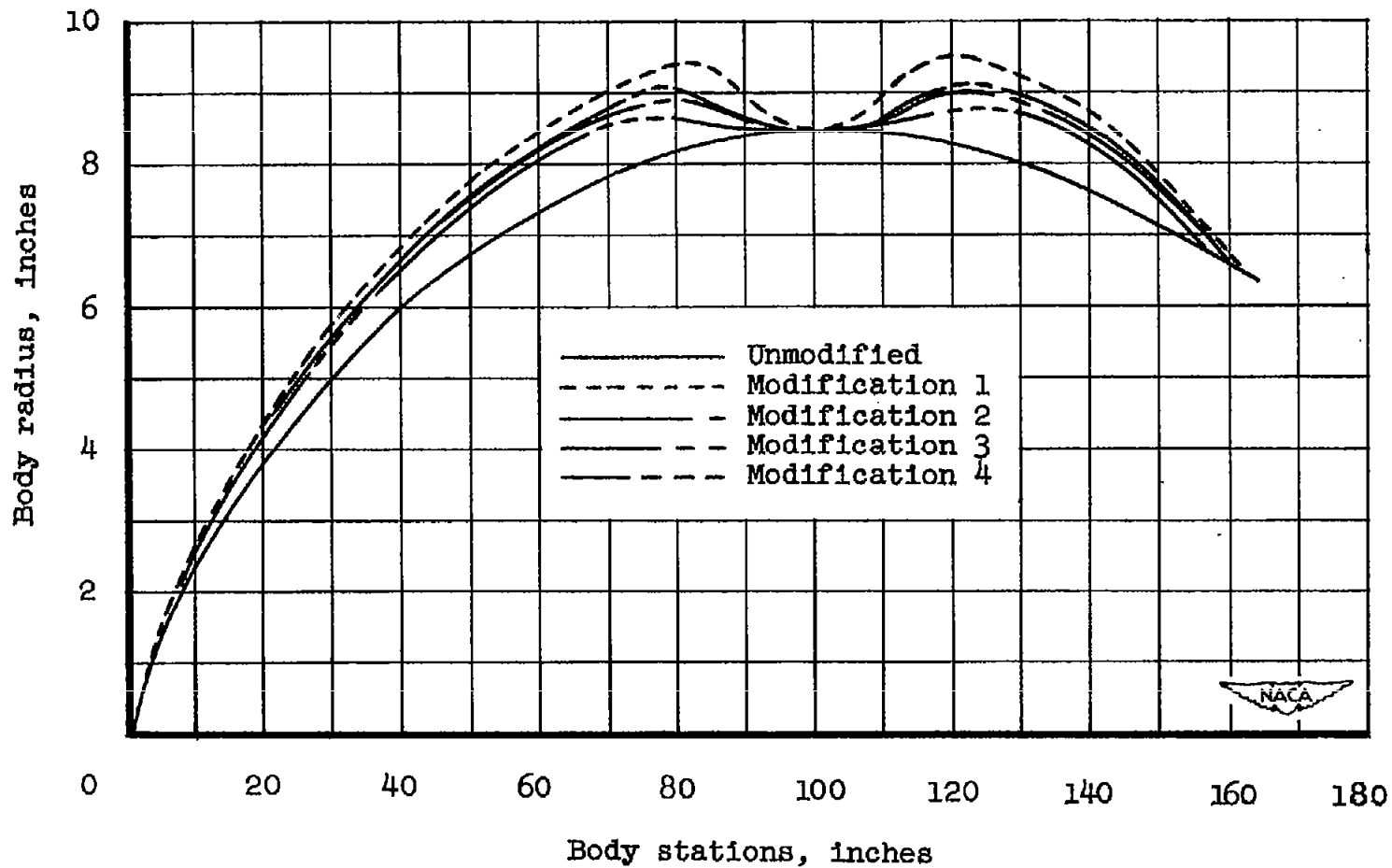
Figure 6.- Comparison of theoretical and experimental increases in drag divided by dynamic pressure.



(a) Calculated drag rise,  $\Delta C_{D0}$ .

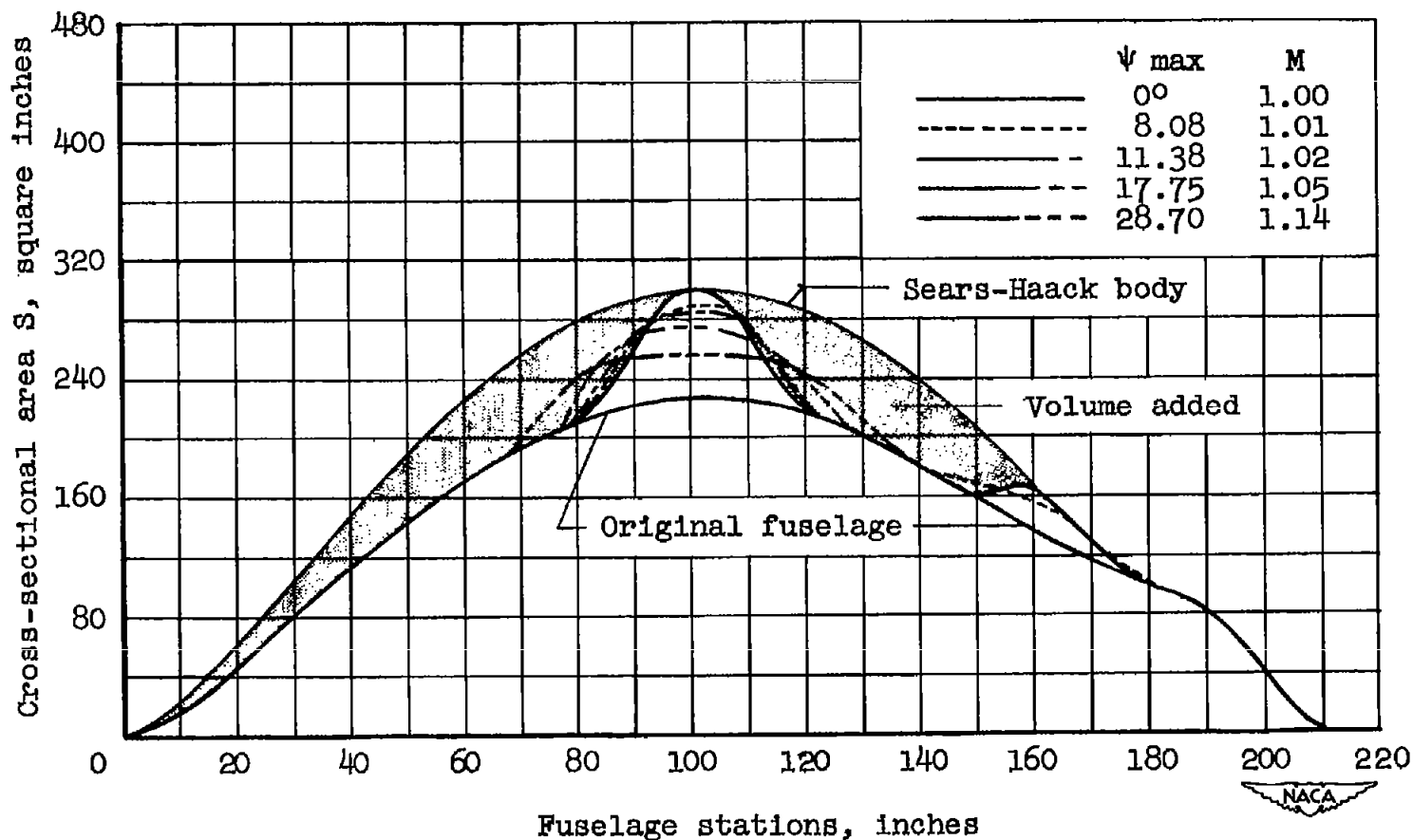
Figure 7.- Comparison of the computed drag rise of model B with the computed values for the same configuration with fuselages of greater volume modified in various ways in an attempt to reduce the drag rise:

- (1) Enlarged body indented for equivalent wing area at  $M = 1.0$
- (2) Enlarged body indented for the arithmetic average of equivalent wing areas ( $S$ ) from  $M = 1.0$  to  $M = 1.14$
- (3) Enlarged body optimized for  $M = 1.05$
- (4) Enlarged body optimized for  $M = 1.14$



(b) Fuselage revisions.

Figure 7.- Concluded.



(a) Modification 1 for  $M = 1.0$ .

Figure 8.- Modifications to the area distribution of model B to reduce drag by adding volume to the fuselage ahead of and behind wing.

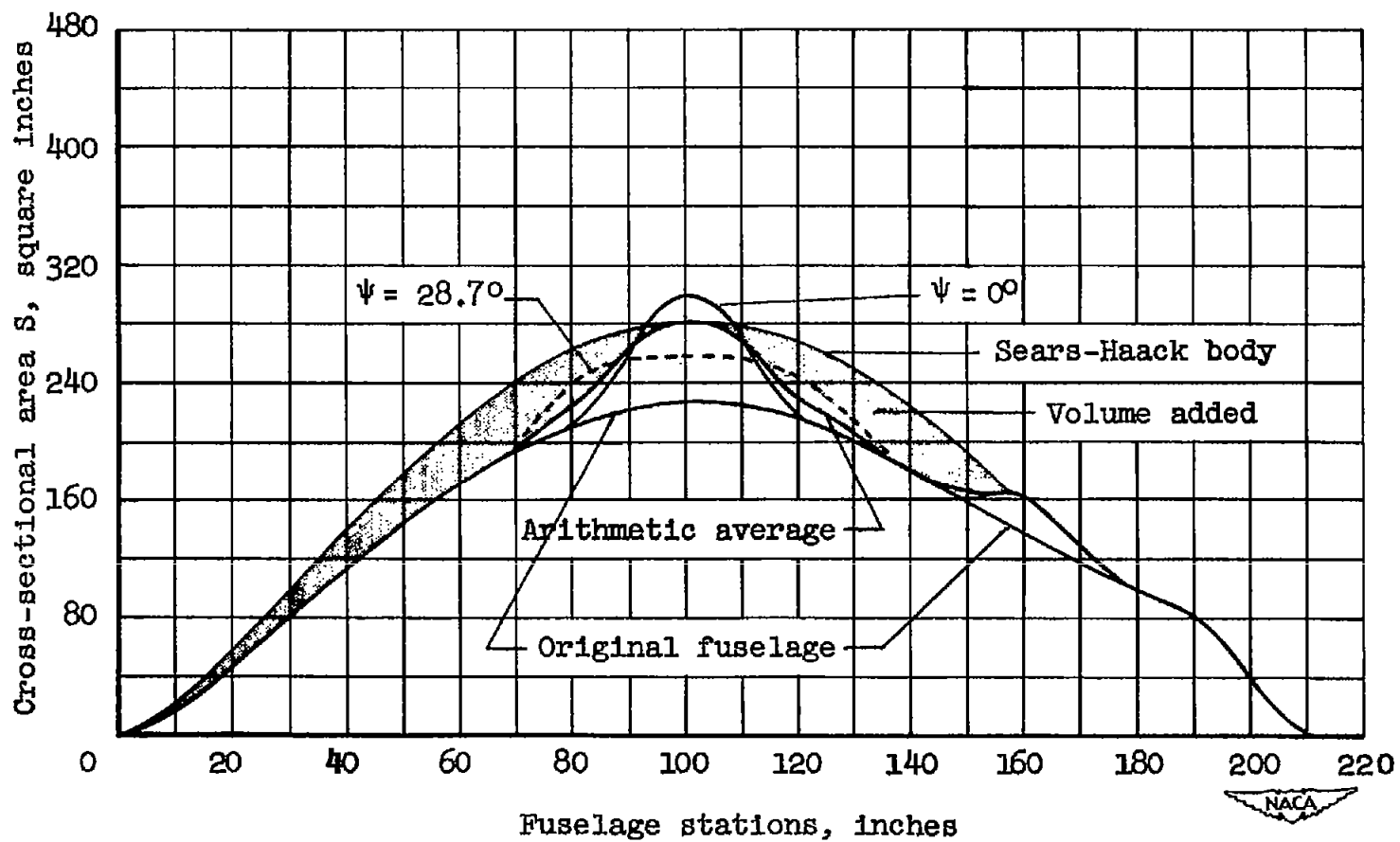
(b) Modification 2 for  $M = 1.0$  to 1.14.

Figure 8.- Concluded.

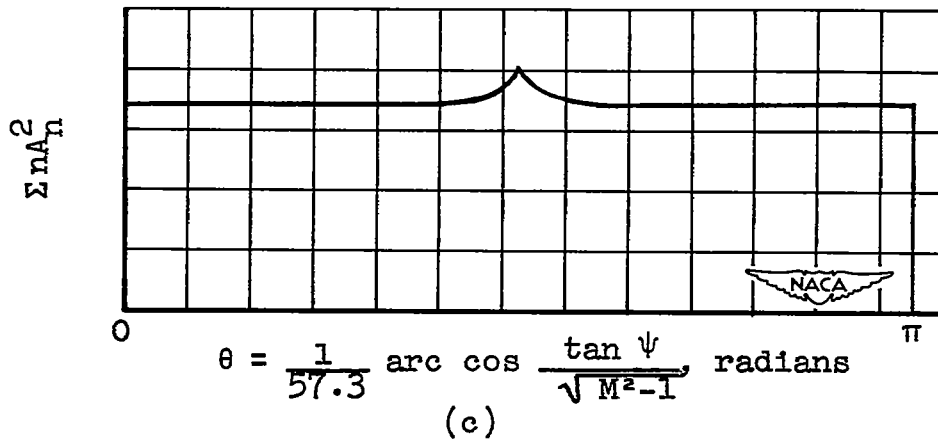
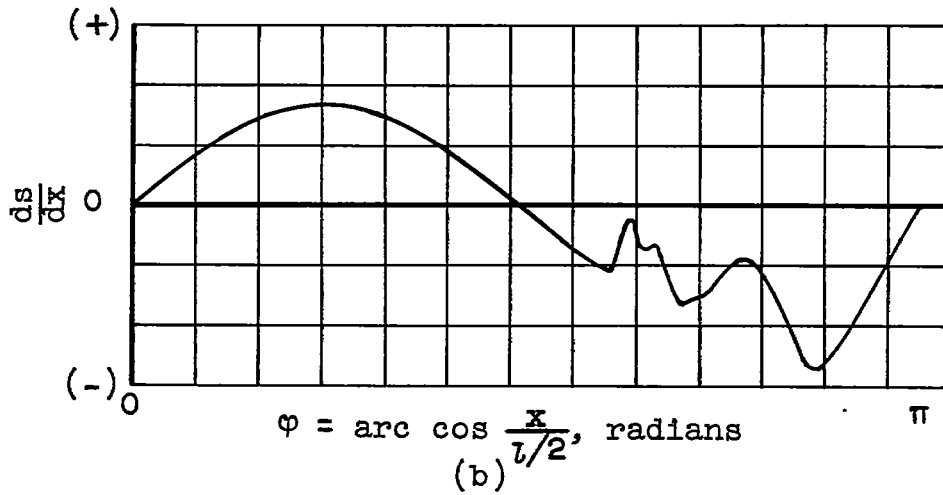
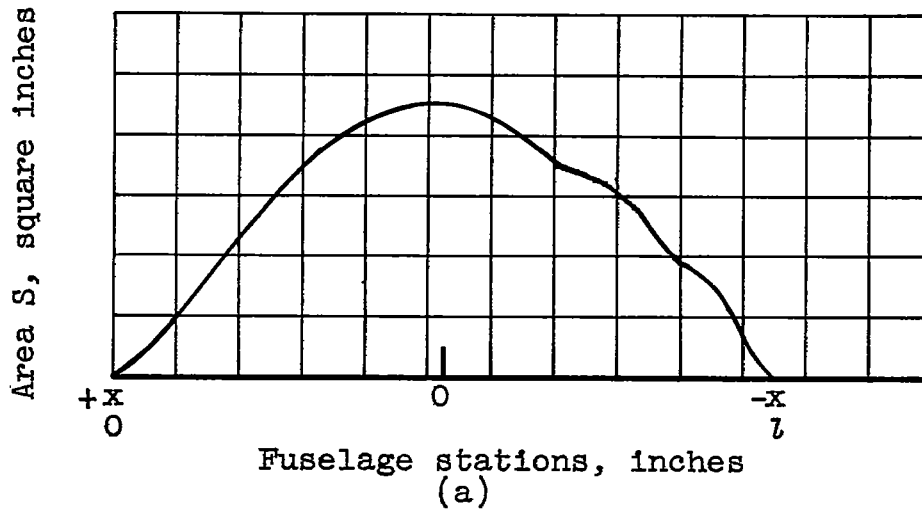


Figure 9.- The three steps in the theoretical solution of the drag rise.  
 For an unsymmetrical configuration, plot C should be made from  $\theta = 0$  to  $\theta = 2\pi$ .